Carbonyl group generation on single-wall carbon nanotubes with nitric acid: A theoretical description

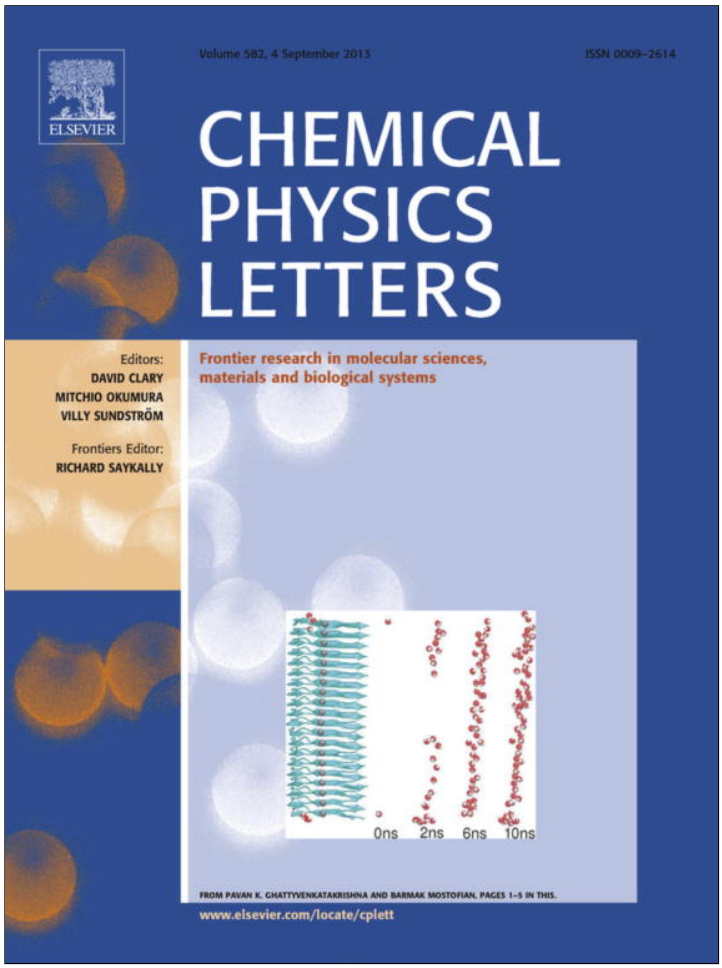

Chemical Physics Letters 582 (2013) 123–128

Contents lists available at ScienceDirect

Chemical Physics Letters

journal homepage: www.elsevier.com/locate/cplett

Carbonyl group generation on single-wall carbon nanotubes with nitric acid: A theoretical description

Antônio M. Da Silva Jr. [a,b], Hélio F. Dos Santos [a,*], Paolo Giannozzi [b,c,*]

[a] NEQC: Núcleo de Estudos em Química Computacional, Departamento de Química, Universidade Federal de Juiz de Fora – UFJF, Juiz de Fora, Minas Gerais 36036-900, Brazil
[b] Department of Chemistry, Physics and Environment, University of Udine, 33100 Udine, Italy
[c] IOM-CNR, 34014 Trieste, Italy

ARTICLE INFO

Article history:
Received 23 May 2013
In final form 24 July 2013
Available online 31 July 2013

ABSTRACT

The initial steps of single-wall carbon nanotube (SWNT) oxidation in nitric acid were studied using a (6,6) supercell with a mono-vacancy defect and employing spin-polarised density functional theory. According to our results, the geometric changes that occur during the process are significantly localised around the vacancy. The carbonyl group generation does not change the metallic nature of the nanosystem. Vibrational thermal corrections calculated using full and partial Hessian vibrational analysis indicated a small contribution to the reaction energy. An overall favourable oxidation pathway is proposed and includes an initial NO_2^+ exothermic electrophilic attack followed by an endothermic oxaziridine formation.

1. Introduction

Due to the chemical inertia of pristine (as-synthesised) carbon nanotubes (CNTs), activation steps are necessary prior to chemical modification [1]. In this sense, oxidative processes should be highlighted as a procedure for purification, removing amorphous carbon and catalyst particles, and surface activation [2]. According to some studies, oxidation occurs preferably at the positions of greatest stress [3–6]. Furthermore, cuts may be made on the tube surface, resulting in open-ended structures or holes in the tube walls [7].

Studies of CNT oxidation may result in many benefits, including (i) improvement in purification processes, (ii) an increase in solubility, (iii) higher chemical reactivity, (iv) new strategies for chemical functionalisation and (v) insights into reaction mechanisms for carbon-based compounds. The interaction of oxidising reagents with CNTs, similar to the oxidation of alkenes, may result in the formation of C–OH, C=O, C–O–C, and O=C–OH functional groups [8,9]. The presence of these groups is often verified by infrared [10] and XPS [11] spectroscopies. A large number of commonly used oxidising agents and their structural consequences have been addressed in the literature. The most common oxidants include air [6], O_2 [12–15], O_3 [16–18], HCl [19], HNO_3 [6,9,20–21], and H_2SO_4/HNO_3 [22]. Each oxidant has intrinsic characteristics and promotes distinct structural changes, which are not completely understood at the molecular level, although these processes date back to the mid-1990s [23]. Nonetheless, the products of these reactions are commonly used as reagents for further chemical processing, for example, for the insertion of amines on the surface of the nanotubes [24]. Among the main oxidising species, the most important are HNO_3 (generally preferred due to its minimal damage on the CNT structures) and H_2SO_4/HNO_3 (this mixture is often more destructive) for liquid phase processes. These species provide purification of as-grown CNTs as well as surface functionalisation with oxygen-containing groups [8,22].

The experimental procedures used to obtain oxidised single-wall carbon nanotube (SWNT) in aqueous solution may involve heating to reflux [21], sonication [25], sonication followed by reflux [26], and hydrothermal autoclaving [8]. For nitric acid, the main products are oxygenated functional groups whose chemical identities and quantities depend on the reaction conditions [21]. According to Gerber et al. [21], for multi-wall carbon nanotube (MWNT) in reflux with an aqueous nitric acid solution (65% v/v) at 393 K, the oxidation reaction starts with the formation of carbonyl groups, which reach a maximum concentration after 1 h. After this, lactones, anhydrides, and carboxylic functional groups are generated. The phenol formation follows a parallel reaction process. Moreover, according to the authors, after four hours, the concentration of surface groups remains nearly constant. After 2 h of reaction, the functional groups are present in the following order: phenol > carbonyl > carboxylic > anhydride > lactone. Despite its chemical importance, the carboxylic group is not dominant. According to Romanos et al. [8], for SWNTs that are hydrothermally treated with an aqueous nitric acid solution (1.25% v/v) in an autoclave at 473 K, a similar order is observed, namely, phenol > carboxylic > lactone > anhydride > carbonyl. For both SWNTs and MWNTs, the phenol group is present in the greatest concentration.

* Corresponding authors. Fax: +55 3232293314.
E-mail addresses: helio.santos@ufjf.edu.br (H.F. Dos Santos), paolo.giannozzi@uniud.it (P. Giannozzi).

0009-2614/$ - see front matter © 2013 Elsevier B.V. All rights reserved.
http://dx.doi.org/10.1016/j.cplett.2013.07.058

According to published studies [22,27,28], for both HNO_3 and H_2SO_4/HNO_3 reagents, the NO_2^+ species acts as the oxidising agent. Cabria et al. [29], using a density functional theory (DFT) solid state approach, observed that NO_2^+ ion binds strongly to a perfect armchair (4,4) SWNT through a charge transfer mechanism, producing significant structural deformities in the vicinity of the adsorbed nitronium ion. The role of the counterion was also investigated (BF_4^-, for a nitronium tetrafluoroborato salt as the oxidising reagent). According to the authors, the anion does not play a primary role in the oxidation of SWNTs. Gerber et al. [21], using nanoflakes with a mono-vacancy defect (usually labelled v1) as a model to mimic CNTs, proposed a possible role of the NO_3^- species (through a nucleophilic attack) in oxidation reactions, thus broadening the range of possibilities for the respective mechanism. That particular vacancy defect has been widely studied in recent years, mainly due to its influence on chemical [30,31] and physical properties [32,33]. In addition, Kim et al. [34] showed that the nitronium hexafluoroantimonate salt (NHFA) can be used as a strong p-type dopant on SWNTs due to a charge transfer process from the SWNT to the NO_2^+ ion. Therefore, these oxidation processes may be useful in the technological applications of CNTs.

Given the importance of the oxidation processes of CNTs, in the present letter, the first step for carbonyl group formation was studied. The system chosen was an armchair (6,6) supercell (labelled a(6,6) hereafter) with a mono-vacancy defect. The computational methodology employed was the periodic boundary conditions (PBC) as implemented in the Quantum ESPRESSO (QE) package [35]. The oxidising agent used was the nitronium ion (NO_2^+) resulting from an acid–base HNO_3 dissociation. Structural, electronic, vibrational, and thermodynamic properties were calculated and discussed.

2. Calculation methodology

All *ab initio* calculations were performed using the Quantum ESPRESSO distribution [35] using spin-polarised DFT with a plane-wave basis set to represent the one-electron wave functions of the Kohn–Sham equations. The Vanderbilt ultrasoft pseudopotentials [36] were used to describe the core electrons, and the PW91 generalised gradient approximation functional [37] was used to describe the exchange–correlation potential for the valence electrons. The additional technical details are summarised in Table 1.

Table 1
Structural and electronic parameters used in the quantum calculations.

General informations about the nanosystem	
Chirality	Armchair (6,6)
Nominal diameter	8.14 Å
Defect	Reconstructed mono-vacancy
Minimum formula	C_{71}[a]($C_{71}H_2O_6N_2$)[b]
Structural parameters used	
$a = b, c$	18.00 Å, 7.39 Å
$\alpha = \beta = \gamma$	90.0°
Self-consistency fied (SCF), ionic and cell convergence thresholds	
SCF	1.0 μRy
Forces for ionic minimization	1.0 mRy a_0^{-1}
Pressures for cell optimization	0.5 kbar
Total energy	0.1 mRy atom^{-1}
Cutoff energies and k-point mesh	
Plane-wave cutoff kinetic energy	25[c](40)[d] Ry
Charge–density cutoff energy	200[c](320)[d] Ry
k-Point mesh ($k_x \times k_y \times k_z$)[e]	$1 \times 1 \times 8$

[a] The isolated and reactive systems, respectively.
[b] The isolated and reactive systems, respectively.
[c] Preprocessing (e.g. structural optimizations) and post-processing (e.g. phonon calculations at gamma point) jobs, respectively.
[d] Preprocessing (e.g. structural optimizations) and post-processing (e.g. phonon calculations at gamma point) jobs, respectively.
[e] Determined by the Monkhorst–Pack procedure.

3. Results and discussion

3.1. The SWNT + HNO_3 reaction model

For the CNT model, a supercell of an armchair (6,6) containing 71 carbon atoms was used. It included a reconstructed vacancy defect (v1) [38] to represent the topological defect, usually produced as-synthesised [3]. A greater supercell would be more representative of the 'real' system but would require too much computational power. Considering the oxidising environment, the first step is to define which species are available in the aqueous nitric acid solution. Initially, the following main processes can be considered Eqs. (1) and (2):

$$\text{Acid-base dissociation}: 2HNO_3 \rightarrow NO_2^+ + NO_3^- + H_2O \; K1 \quad (1)$$

$$\text{Acid dissociation}: HNO_3 + H_2O \rightarrow H_3O^+ + NO_3^- \; K2 \quad (2)$$

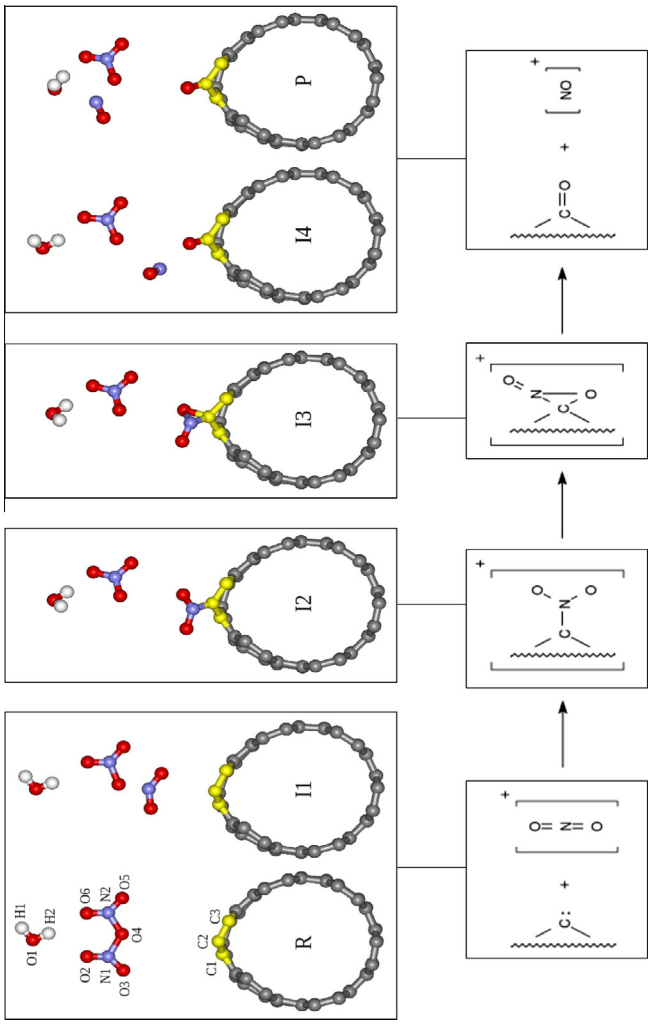

Figure 1. A schematic representation of the proposed chemical process (a transverse section of the structures are depicted). Only the highlighted carbon atoms (yellow colour) were included in the partial Hessian vibrational analysis. (For interpretation of the references to colour in this figure legend, the reader is referred to the web version of this article.)

Table 2
Optimized bond lengths (r, in Å), angles (<, in degree) and dihedrals (d, in degrees) for the species shown in Figure 1.

Structural parameter	Structure					
	R	I1	I2	I3	I4	*P*
r_{CC}	1.43	1.43	1.43	1.43	1.43	1.43
$r_{C2C(1,3)}$[a]	1.38	1.38	1.44	1.49	1.48	1.49
r_{C2N1}	6.30	3.71	1.44	1.45	3.22	6.19
r_{C2O3}	5.67	3.18	2.31	1.46	1.23	1.22
r_{N1O3}	2.27	1.19	1.25	1.56	2.36	5.24
r_{N1O2}	2.27	1.19	1.26	1.23	1.44	1.44
r_{N1O4}	1.60	1.71	4.19	4.10	3.02	1.85
$r_{N2O(4,5,6)}$	1.31	1.29	1.26	1.26	1.27	1.28
r_{O4H2}	4.13	3.71	3.54	3.55	3.22	2.85
$r_{O6HChe1}$	3.76	3.58	1.99	2.00	3.19	3.18
$<_{C1C2C3}$	119.5	118.8	113.8	107.4	109.1	108.4
$<_{C2O4N1}$	113.8	5.9	12.7	14.4	37.1	119.4
$<_{O2N1O3}$	134.9	137.5	125.1	120.9	104.7	73.2
$d_{O2N1N2O6}$	0.9	0.9	2.6	6.9	65.0	156.2
RMSD[b]	0.0	0.1	0.1	0.1	0.1	0.1

[a] average value for the r_{C2C1} and r_{C2C3} bond lengths.
[b] Root-mean-square deviation of the carbon atoms Cartesian coordinates with respect to the isolated *a*(6,6), except the C1, C2 and C3 atoms.

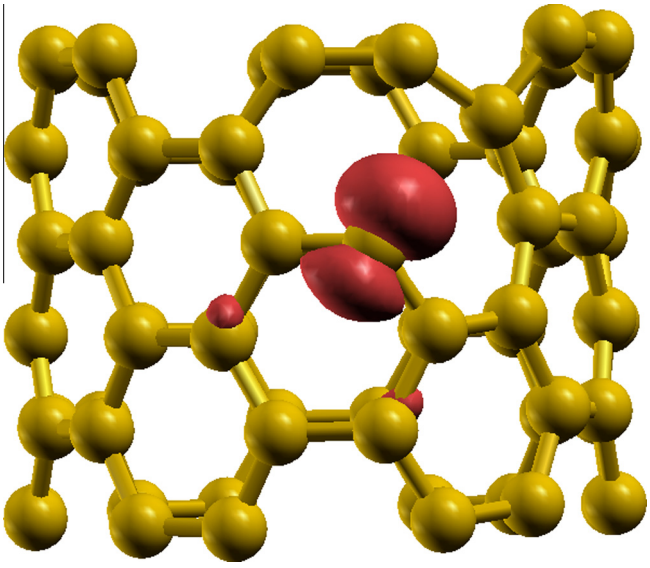

Figure 2. Representation of the isolated a(6,6)-v1 supercell and its spin polarisation (*electronic density* (*up*) – *electronic density* (*down*); isovalue = 0.003 e/a.u.^{3}).

There may be at least five different species in solution (NO_2^+, H_3O^+, HNO_3, H_2O, and NO_3^-). Assuming that HNO_3 is a strong acid, K2 is significantly greater than K1 (in the usual experimental ranges of temperature and pressure); therefore, it is possible to assume the following order of chemical availability: H_2O (solvent) >> NO_3^- > H_3O^+ > NO_2^+ >> HNO_3. Considering the significant passivity of water with respect to the non-chemically modified SWNTs [39,40], the NO_3^-, H_3O^+ and NO_2^+ species should be taken into account. For the oxygen transfer processes, the NO_2^+ nucleophilic species is more susceptible to reduction reactions (nitronium → nitrosonium ion). Thus, the chemical process used consisted of a periodic a(6,6) interacting with the species derived from Eq. (1) as shown in Eq. (3).

$$C_{71((6,6)-v1)} + NO_2NO_3.H_2O \rightarrow C_{71}O_{((6,6)-v1)} + NONO_3.H_2O \quad (3)$$

The present reaction model does not rule out other chemical possibilities. It is just one possible method of accessing the experimentally obtained carbonyl groups as part of a more complex global process.

3.2. Structural analysis

The proposed chemical process is depicted in Figure 1. For every reactive species, the atomic coordinates of the oxygen labelled O4 were fixed at a C2–O4 of approximately 5.5 Å. According to our reaction model, the *R* → I1 rotation ($<_{C2O4N1}$ = 113.8 → 5.9 degree; see Table 2) allowed the approach of the nitronium ion into the reactive site on the tube surface (C2), and the r_{C2N1} distance decreased from 6.30 to 3.71 Å. The next step considered is the migration of the NO_2^+ ion from the solute environment onto the nanotube surface under an electrophilic attack (I1 → I2). The new C–N bond of 1.44 Å implies a decreased distance of the N–O bonds (NO_2^+) from 2.27 to 1.26 Å. Following the reaction pathway, after the electrophilic attack, the next step is an oxygen transfer process that is conducted through an oxaziridine-derivative [41] formation (I3). Due to its strain and the two strong electronegative oxygen atoms bound to the nitrogen, the oxaziridine ring may open following the Vidal nitrogen transfer mechanism [42], releasing a nitrosonium ion (I4). The carbonyl product *P* has a slightly greater separation between the ionic species and the nanosurface than the I4 species (I4: rN1O3 = 2.36 Å; *P*: rN1O3 = 5.24 Å). The chemical modification is significantly localised, as indicated by the root-mean-square deviation (RMSD) of the nonreactive carbon atom coordinates with respect to the isolated a(6,6) (smaller than 0.1 Å; see Table 2).

3.3. Electronic analysis

The isolated a(6,6)-v1 (Figure 2), despite its chemical similarity (two dangling bonds), does not display the electronic characteristics of conventional carbenes. This class of compounds usually shows singlet or triplet multiplicity and null charge [43]. However, according to our results, the divalent carbon atom depicted in Figure 2 has both an atomic charge (in e) and a magnetisation (in μB/cell) equal to 0.5. Analogous magnetic behaviour was found by Yuchen et al. for a short a(6,6) supercell [44]. Some similarities to carbenes arise when the ionic species are present in the supercell (*R* species; Figure 1), which changes these properties to a null charge and singlet multiplicity. It is important to make clear that the absolute value of magnetization depends on the size of unit cell and might be doubtful for small unit cell as that used here. Nevertheless, the same size of unit cell was used for all reactive species in the present study and, therefore, the magnetization might be analysed as relative quantity throughout the reaction pathway.

The studies addressing with CNT oxidation usually focus on nanostructures [45,46] and overlook the by-products. Therefore, the chemical identities sometimes become unclear. In general, nitrogen-based compounds are not found in appreciable quantities on the nanostructures after the chemical process. According to our model and considering a non-solvated medium, the nitrogenated compound to be released is the NO^{x+} species. Eq. (4) illustrates the process with *R* as the reactant and *P* as the product (see Figure 1). Despite the small calculated fractional charge, a qualitative interpretation may be performed. During the process, a residual charge is transferred from the carbon nanotube.

$$C_{71((6,6)-v1)^{0.0}} + NO_2^{0.2+}NO_3^{0.2-}.H_2O^{0.0} \rightarrow C_{71}O_{((6,6)-v1)^{0.1+}} + NO^{0.3+}NO_3^{0.4-}.H_2O^{0.0} \quad (4)$$

The electronic states change with the oxidation of each structure. Figure 3a illustrates the density of states (DOS) plotting for all species. The metallic nature of the isolated defective tube [47]

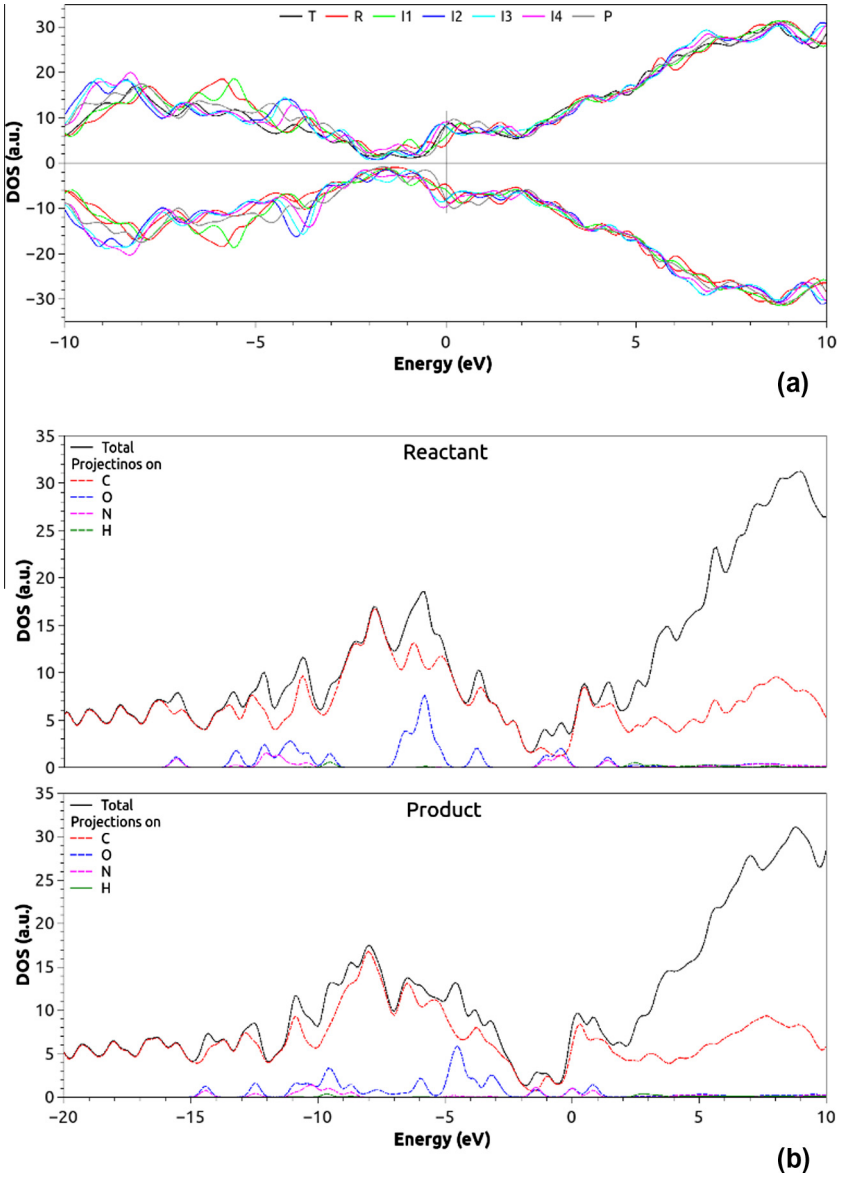

Figure 3. Spin-resolved DOS plotting for all species along the oxidative process (T: isolated a(6,6)-v1) and spin-up PDOS for the reactant (a) and product (b).

(black line) remains unchanged during each stage of the oxygen transfer process. The most substantial modifications occur below the Fermi level (FL) with the spin up and down differentiations highlighted only for the I2, I3 and I4 species (greater total magnetisations, equal to 1.5, 1.6 and 1.2 μ_B/cell, respectively). Figure 3b shows the projected density of states (PDOS) plotting for the reactant and product. For both structures, the carbon atom contributions are dominant. However, for a small range close to the FL, the oxygen and nitrogen atom contributions are greater than the carbon ones. In addition, a greater contribution from the heteroatoms (O and N) to the Fermi level electronic states may be observed for the product (Figure 3b).

3.4. Vibrational and thermodynamic analysis

For a system containing N atoms, the full Hessian vibrational analysis (FHVA) considers a $3\,N \times 3\,N$ Hessian matrix of which the mass-weighting and diagonalisation yield $3\,N$ frequencies and normal modes. This standard normal modes analysis becomes prohibitive for large and complex systems due to the high computational cost required. In contrast, the partial Hessian vibrational analysis (PHVA) reduces the computational effort by calculating only selected/relevant normal modes for a specific application [48]. It enables the choice of a different number of 'free' (N_{free}) and 'fixed' (N_{fixed}) atoms to be or not be displaced (labelled as $\{N_{free}, N_{fixed}\}$ from henceforth) [49]. The 'frozen' atoms are modelled as infinite masses during the frequency calculation and do not contribute directly to the vibrational modes, despite their influence over each original Hessian matrix component and post-SCF calculation. The PHVA does not alter the description of the potential energy surface (PES) but reduces the Hessian matrix to a $3N_{free} \times 3N_{free}$ dimension and yields $3N_{free}$ eigenvalues and eigen vectors. To evaluate the thermal contributions to the total energy during each stage of the chemical process, we used a {13, 68} scheme, as depicted in Figure 1. The portion coloured as gray was kept fixed, and the remaining portion (C-yellow, H, N, and O atoms) was free.

To calculate the thermodynamic corrections from the vibrational contributions, the methodology described by Ferreira et al. [50] was used. For the reactant (R) and product (P), the FHVA and PHVA approaches were checked (Figure 4). With respect to the harmonic frequencies and atomic displacements, good

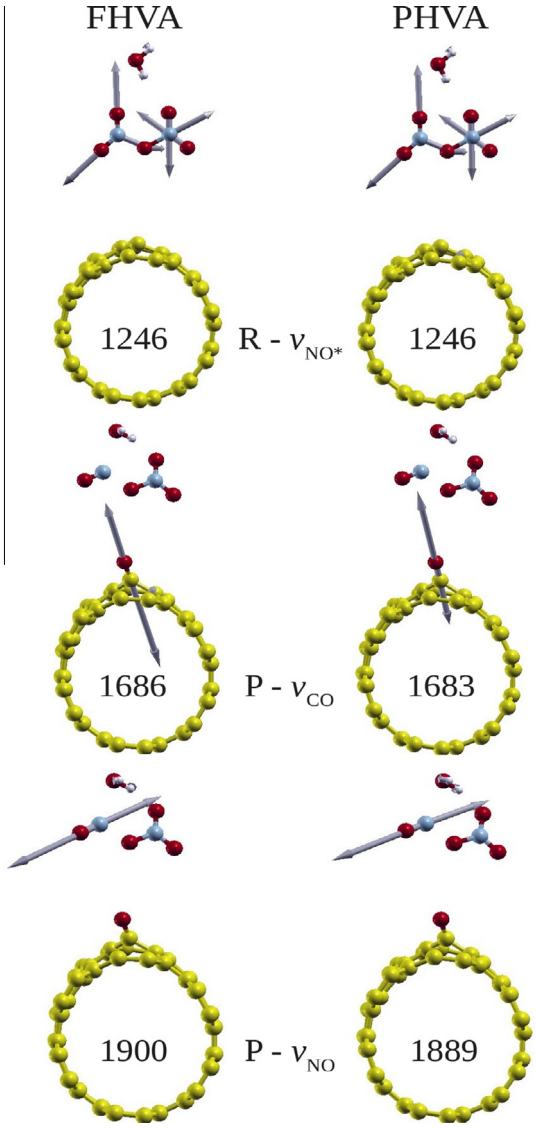

Figure 4. Atomic displacements and ν_{NO*} (in the NO_2^+ and NO_3^- species), ν_{CO} and ν_{NO} stretching frequencies calculated using the full and partial Hessian vibrational analysis for the reactant (top) and product (bottom).

agreement between the corresponding normal modes was found. To illustrate this finding, Figure 4 shows the NO stretching (in the NO_2^+ and NO_3^- species) for the *R* species, and the CO (carbonyl) and NO (nitrosonium ion) stretching are shown for the *P* species. For the selected reactant vibrational properties, there is no visible difference between the harmonic frequencies and the atomic displacements. For the product, the bond stretching presented small differences, less than 3 cm^{-1} between the FHVA and PHVA corresponding modes (see Figure 4). Despite the good agreement between FHVA e PHVA approaches, it should bear in mind that only hard normal modes are calculated and, therefore, the reduced Hessian diagonalization gives satisfactory frequencies. Nonetheless, thermodynamic properties, mainly entropy, are quite sensitive to the soft normal modes and thus, FHVA might be necessary for accurate prediction of absolute values. This drawback is minimised when reaction energies involving isomer species (monomolecular process) are desired due cancelation of contributions from low frequency modes (soft modes) which should be strongly delocalised. For the process investigated in the present letter, ΔA for the global reaction ($R \rightarrow P$) differs by only 2.6 kcal mol^{-1} when FHVA and PHVA approaches are used, corresponding to ~3% of the total Δ*A* values.

Table 3
Thermodynamic properties calculated for each stage along the oxidative process (T = 298.15 K).

Parameters (kcal mol^{-1})	Structure						
	PHVA[a]						FHVA[b]
	$R \rightarrow$ I1	I1 → I2	I2 → I3	I3 → I4	I4 → P	$R \rightarrow P$	$R \rightarrow P$
ΔE	−1.4	−32.4	21.8	−42.3	−15.9	−70.2	−70.2
ΔU	−1.4	−32.5	21.8	−42.1	−16.1	−70.3	−70.4
−TΔS	0.2	1.3	−1.4	4.3	−4.3	0.1	−2.4
ΔA	−1.2	−31.2	20.4	−37.8	−20.7	−70.2	−72.8

[a] Partial hessian vibrational analysis.
[b] Full hessian vibrational analysis.

The PHVA was used to calculate the vibrational contributions to the reaction energies, as depicted in Table 3. The process starts with a rotation of the nitrogenated cation ($R \rightarrow$ I1, ΔA = −1.2 kcal mol^{-1}) followed by a much more exergonic electrophilic attack on the tube (I1 → I2, ΔA = −31.2 kcal mol^{-1}). As the oxygen-transfer is the focus, a rearrangement that requires 20.4 kcal mol^{-1} (I2 → I3, oxaziridine formation) is necessary. This endergonic process is balanced by a strong exergonic ring opening process (I3 → I4, nitrosonium production; −37.8 kcal mol^{-1}) and relaxation into the more ionic environment (I4 → P, −20.7 kcal mol^{-1}; see Table 3). The total PHVA-Helmholtz free energy (PHVA-ΔA) for the $R \rightarrow P$ process is −70.2 kcal mol^{-1}. From the values in Table 3 we note that the dominant contributions come from the internal energies (ΔE and ΔU), and the TΔS portion corresponds only to 4–21%. Lastly, the overall profile for the reaction pathway suggests the formation of the oxaziridine ring (I2 → I3) as the 'rate determining step', even though the transition state (TS) has not been found. The I3 species was characterized as a minimum point on the potential energy surface with all PHVA vibrational modes predicted to be real (see Figure S1 as Supplementary Material). Nevertheless, we suggest that the true TS must be close in energy and structure to the I3 intermediate and, therefore, the free energy barrier (ΔA) might be extrapolated for carbonyl generation around 20 kcal mol^{-1}.

4. Concluding remarks

In the present letter, spin-polarised DFT calculations were conducted for the structural, electronic, vibrational and energetic analysis of a modelled SWNT + HNO_3 chemical reaction. The system studied was an armchair (6,6) supercell with a mono-vacancy defect, considering a reaction environment of NO_2^+, NO_3^-, and H_2O from the acid–base HNO_3 dissociation. As the reaction progresses, the carbonyl group generation does not change the metallic nature of the nanosystem and, depending on the reaction stage, the density of states might increase or decrease on the Fermi level. As predicted by the root-mean-square deviation of the passive carbon atom coordinates (not greater than 0.1 Å, with respect to the isolated a(6,6)) and from the vibrational thermal contribution using the full and partial Hessian vibrational analysis (FHVA and PHVA, respectively), oxygen incorporation is a significantly localised process. There were only small differences between the atomic displacements and the harmonic frequencies predicted for the *R* and *P* species by both the FHVA and the PHVA models. An overall favourable oxidation (FHVA-ΔA = 72.8 kcal mol^{-1}) was calculated, and the predicted thermal contributions corresponded to only 4% of the total energy. The chemical process included an initial NO_2^+ exothermic electrophilic attack followed by the endothermic oxaziridine formation. We believe the results reported in this study

might add to the molecular description of oxidation of CNT and assist the experimentalist in the characterization of intermediate species.

Acknowledgments

The authors (HFDS and AMDS) would like to thank the Brazilian agencies CNPq, CAPES and FAPEMIG for financial support. AMDS would like to thank the CAPES for the PDSE graduate scholarship (process 6789-11-0). In addition, HFDS and AMDS are grateful to Hélio Anderson Duarte and his Research Group in Theoretical Inorganic Chemistry for providing computational resources for the vibrational frequencies analysis.

Appendix A. Supplementary data

Supplementary data associated with this article can be found, in the online version, at http://dx.doi.org/10.1016/j.cplett.2013.07.058.

References

[1] P.-X. Hou, C. Liu, H.-M. Cheng, Carbon 46 (2008) 2003.
[2] D. Tasis, N. Tagmatarchis, A. Bianco, M. Prato, Chem. Rev. 106 (2006) 1105.
[3] A. Barinov, L. Gregoratti, P. Dudin, S. La Rosa, M. Kiskinova, Adv. Mater. 21 (2009) 1916.
[4] Y. Fan, B.R. Goldsmith, P.G. Collins, Nat. mater. 4 (2005) 906.
[5] H.F. Bettinger, J. Phys. Chem. B 109 (2005) 6922.
[6] X. Li, J. Niu, J. Zhang, H. Li, Z. Liu, J. Phys. Chem. B 107 (2003) 2453.
[7] J. Li, Y. Zhang, Appl. Surf. Sci. 252 (2006) 2944.
[8] G.E. Romanos et al., J. Phys. Chem. C 115 (2011) 8534.
[9] J. Zhang et al., J. Phys. Chem. B 107 (2003) 3712.
[10] D.B. Mawhinney, V. Naumenko, A. Kuznetsova, J.T. Yates, J. Liu, R.E. Smalley, J. Am. Chem. Soc. 122 (2000) 2383.
[11] T.I.T. Okpalugo, P. Papakonstantinou, H. Murphy, J. Mclaughlin, N.M.D. Brown, Carbon 43 (2005) 153.
[12] A.M. Da Silva, G.M.A. Junqueira, C.P.A. Anconi, H.F. Dos Santos, J. Phys. Chem. C 113 (2009) 10079.
[13] P. Liu, F. Arai, T. Fukuda, Appl. Phys. Lett. 89 (2006) 113104.
[14] M.A. Hamon, K.L. Stensaas, M.A. Sugar, K.C. Tumminello, A.K. Allred, Chem. Phys. Lett. 447 (2007) 1.
[15] P. Giannozzi, R. Car, G. Scoles, J. Chem. Phys. 118 (2003) 1003.
[16] J.M. Simmons et al., J. Phys. Chem. B 110 (2006) 7113.
[17] E. Najafi, J.-Y. Kim, S.-H. Han, K. Shin, Colloids Surf. A 284–285 (2006) 373.
[18] M. Li, M. Boggs, T.P. Beebe, C.P. Huang, Carbon 46 (2008) 466.
[19] V. Datsyuk et al., Carbon 46 (2008) 833.
[20] Y. Li et al., Nanotechnology 15 (2004) 1645.
[21] I. Gerber et al., Chem. Eur. J. 17 (2011) 11467.
[22] C.-M. Yang et al., J. Phys. Chem. B 109 (2005) 19242.
[23] S.C. Tsang, Y.K. Chen, P.J.F. Harris, M.L.H. Green, Nature 372 (1994) 159.
[24] T. Ramanathan, F.T. Fisher, R.S. Ruoff, L.C. Brinson, Chem. Mater. 17 (2005) 1290.
[25] M.N. Tchoul, W.T. Ford, G. Lolli, D.E. Resasco, S. Arepalli, Chem. Mater. 19 (2007) 5765.
[26] H. Yu, Y. Jin, F. Peng, H. Wang, J. Yang, J. Phys. Chem. C 112 (2008) 6758.
[27] K.H. An et al., J. Electron. Mater. 35 (2006) 235.
[28] K.H. An et al., J. Am. Chem. Soc. 127 (2005) 5196.
[29] I. Cabria, M.J. López, J.A. Alonso, J. Chem. Phys. 128 (2008) 214703.
[30] J. Robles, M.J. López, J.A. Alonso, Eur. Phys. J. D 61 (2011) 381.
[31] A. Galano, M. Francisco-marquez, A. Martínez, J. Phys. Chem. C 114 (2010) 8302.
[32] R.H. Poelma, H. Sadeghian, S. Koh, G.Q. Zhang, Microelectron. Reliab. 52 (2012) 1279.
[33] Z.E. Zadeh, M. Yadollahpour, S. Ziaei-Rad, F. Karimzadeh, Comp. Mater. Sci. 63 (2012) 12.
[34] K.K. Kim, J.J. Bae, S.M. Kim, H.K. Park, K.H. An, Y.H. Lee, Phys. Status Solidi B 246 (2009) 2419.
[35] P. Giannozzi et al., J. Phys. Condens. Matter 21 (2009) 395502.
[36] D. Vanderbilt, Phys. Rev. B 41 (1990) 7892.
[37] J.P. Perdew, Y. Wang, Phys. Rev. B 45 (1992) 13244.
[38] J.E. Padilha, R.G. Amorim, A.R. Rocha, A.J.R. da Silva, A. Fazzio, Solid State Commun. 151 (2011) 482.
[39] J.A. Thomas, A.J.H. McGaughey, J. Chem. Phys. 128 (2008) 084715.
[40] M.F. Islam, E. Rojas, D.M. Bergey, A.T. Johnson, A.G. Yodh, Nano Lett. 3 (2003) 269.
[41] W.D. Emmons, J. Am. Chem. Soc. 79 (1957) 5739.
[42] J. Vidal, S. Damestoy, L. Guy, J.-C. Hannachi, A. Aubry, A. Collet, Chem. Eur. J. 3 (1997) 1691.
[43] D. Bourissou, O. Guerret, F.P. Gabbaı, G. Bertrand, Chem. Rev. 100 (2000) 39.
[44] Y. Ma, P.O. Lehtinen, A.S. Foster, R.M. Nieminen, New J. Phys. 6 (2004) 68.
[45] Y.-C. Chiang, W.-H. Lin, Y.-C. Chang, Appl. Surf. Sci. 257 (2011) 2401.
[46] J. Chen, Q. Chen, M. Qing, J. Colloid Interface Sci. 370 (2012) 32.
[47] W. Orellana, P. Fuentealba, Surf. Sci. 600 (2006) 4305.
[48] A. Ghysels, V.V. Speybroeck, E. Pauwels, S. Catak, B.R. Brooks, D.V. Neck, M. Waroquier, J. Comp. Chem. 31 (2010) 994.
[49] B.A. De Moor, A. Ghysels, M.-F. Reyniers, V.V. Speybroeck, M. Waroquier, G.B. Marin, J. Chem. Theory Comput. 7 (2011) 1090.
[50] A.R. Ferreira et al., J. Solid State Chem. 184 (2011) 1105.